Mon. Not. R. Astron. Soc. **000**, 1–15 (2014) Printed 25 June 2014 (MN LATEX style file v2.2)

Non-linear galactic dynamos: A toolbox

Luke Chamandy,[1⋆] Anvar Shukurov,[2,1] Kandaswamy Subramanian,[1] Katherine Stoker[2]
[1] *Inter-University Centre for Astronomy and Astrophysics, Post Bag 4, Ganeshkhind, Pune 411007, India*
[2] *School of Mathematics & Statistics, Newcastle University, Newcastle upon Tyne NE1 7RU*

arXiv:1403.2562v2 [astro-ph.GA] 24 Jun 2014

25 June 2014

ABSTRACT

We compare various models and approximations for non-linear mean-field dynamos in disc galaxies to assess their applicability and accuracy, and thus to suggest a set of simple solutions suitable to model the large-scale galactic magnetic fields in various contexts. The dynamo saturation mechanisms considered are the magnetic helicity balance involving helicity fluxes (the dynamical α-quenching) and an algebraic α-quenching. The non-linear solutions are then compared with the marginal kinematic and asymptotic solutions. We also discuss the accuracy of the no-z approximation. Although these tools are very different in the degree of approximation and hence complexity, they all lead to remarkably similar solutions for the mean magnetic field. In particular, we show that the algebraic α-quenching non-linearity can be obtained from a more physical dynamical α-quenching model in the limit of nearly azimuthal magnetic field. This suggests, for instance, that earlier results on galactic disc dynamos based on the simple algebraic non-linearity are likely to be reliable, and that estimates based on simple, even linear models are often a good starting point. We suggest improved no-z and algebraic α-quenching models, and also incorporate galactic outflows into a simple analytical dynamo model to show that the outflow can produce leading magnetic spirals near the disc surface. The simple dynamo models developed are applied to estimate the magnetic pitch angle and the arm-interarm contrast in the saturated magnetic field strength for realistic parameter values.

Key words: magnetic fields – MHD – dynamo – galaxies: magnetic fields – galaxies: spiral – galaxies: structure

1 INTRODUCTION

The mean-field dynamo theory provides an appealing explanation of the presence and structure of large-scale magnetic fields in disc galaxies (Ruzmaikin et al. 1988; Beck et al. 1996; Brandenburg & Subramanian 2005; Shukurov 2005; Kulsrud & Zweibel 2008). The dynamo time scale is shorter than the galactic lifetime, and the energy densities of the large-scale galactic magnetic fields and interstellar turbulence are observed to be of the same order of magnitude. It is thus plausible that the galactic large-scale dynamos are normally in a non-linear, statistically steady state. Recent progress in dynamo theory has lead to physically motivated non-linear models where the steady state is achieved through the magnetic helicity balance in the dynamo system (reviewed by Brandenburg & Subramanian 2005; Blackman 2014). To avoid a catastrophic suppression of the mean induction effects of turbulence, the magnetic helicity of random magnetic fields should be removed from the system. In galaxies, this can be achieved through the advection of magnetic fields from the disc to the halo by the galactic fountain or wind (Shukurov et al. 2006; Sur et al. 2007), diffusive flux (Kleeorin et al. 2000, 2002) and helicity flux relying on the anisotropy of the interstellar turbulence (Vishniac & Cho 2001; Vishniac & Shapovalov 2014) (see Sur et al. 2007, for an application to galaxies). The first of these mechanisms is the simplest in physical and mathematical terms, and involves galactic parameters that are reasonably well constrained observationally.

Most of the earlier analytical and numerical results in the non-linear mean-field disc dynamo theory rely on a much simpler form of non-linearity in the dynamo equations, the so-called algebraic α-quenching that is based on a simple, explicit form of the dependence of the dynamo parameters, usually the α-coefficient, on the magnetic field. In a thin layer, such as a galactic or accretion disc, this allows one to obtain a wide range of analytical and straightforward numer-

⋆ E-mail: luke@iucaa.ernet.in; anvar.shukurov@ncl.ac.uk; kandu@iucaa.ernet.in; k.j.stoker@googlemail.com

© 2014 RAS

ical solutions using simple and yet accurate approximations (e.g., Shukurov 2007). One of the advantages of the resulting theory of galactic magnetic fields is that all its essential parameters can be expressed in terms of observable quantities (the angular velocity of rotation, thickness of the gas layer, turbulent velocity, etc.). As a result, theory of galactic magnetic fields has been better constrained and verified by direct comparison with observations than, arguably, any other astrophysical dynamo theory. Such comparisons require relatively simple, preferably analytical, approximations to the solutions of the dynamo equations. In this paper we consider numerical solutions of thin-disc dynamo equations with a dynamic non-linearity involving magnetic helicity balance and compare them with a wide range of simpler solutions to develop a set of accessible tools to facilitate applications of the theory.

The paper is organized as follows. In Sections 2-4, we present the theoretical background and a review of each of the approximations discussed. This is followed by a detailed comparison of the solutions resulting from various physical and mathematical approximations in Section 5. In particular, in Section 6 we provide an in-depth comparison of the dynamical and algebraic non-linearities. Our overall conclusion is that the earlier, simple models, when applied judiciously, reproduce comfortably well solutions with the dynamical non-linearity. Section 7 provides examples of applications of the toolbox, namely the magnetic pitch angle problem and the spiral arm-interarm contrasts in magnetic field. We present a summary and general conclusions in Section 8. The details of the asymptototic solutions studied, namely the perturbation and no-z solutions, are given in Appendices A and B, respectively.

Throughout this paper, we use cylindrical polar coordinates (r, ϕ, z) with the origin at the disc centre and the z-axis aligned with the angular velocity of rotation $\boldsymbol{\Omega}$.

2 NONLINEAR MEAN-FIELD DYNAMOS

Magnetic field averaged over scales exceeding the turbulent scales, the mean magnetic field $\overline{\boldsymbol{B}}$, is governed by the induction equation suitably averaged in a mirror-asymmetric random flow (Moffatt 1978; Krause & Rädler 1980):

$$\frac{\partial \overline{\boldsymbol{B}}}{\partial t} = \nabla \times \left(\overline{\boldsymbol{U}} \times \overline{\boldsymbol{B}} + \alpha \overline{\boldsymbol{B}} - \eta_{\rm t} \nabla \times \overline{\boldsymbol{B}} \right) \qquad (1)$$

where overbar denotes averaged quantities, $\eta_{\rm t}$ is the magnetic diffusivity (dominated by the turbulent diffusion), $\boldsymbol{B}$ is the magnetic field and $\boldsymbol{U}$ is the velocity field, both assumed to be separable into the mean and random parts,

$$\boldsymbol{U} = \overline{\boldsymbol{U}} + \boldsymbol{u}, \quad \boldsymbol{B} = \overline{\boldsymbol{B}} + \boldsymbol{b}\,,$$

with $\overline{\boldsymbol{u}} = \boldsymbol{0}$ and $\overline{\boldsymbol{b}} = \boldsymbol{0}$.

Following Pouquet et al. (1976); Kleeorin et al. (1995); Blackman & Field (2000), the α-effect in Eq. (1) is represented as the sum of kinetic and magnetic contributions,

$$\alpha = \alpha_{\rm k} + \alpha_{\rm m},$$

where $\alpha_{\rm k} = -\tau \overline{\boldsymbol{u} \cdot \boldsymbol{\nabla} \times \boldsymbol{u}}/3$ is the 'kinetic' part related to the mean helicity of the random flow $\overline{\boldsymbol{u} \cdot \boldsymbol{\nabla} \times \boldsymbol{u}}$, and $\alpha_{\rm m} = \tau \overline{\boldsymbol{b} \cdot \boldsymbol{\nabla} \times \boldsymbol{b}}/(12\pi\rho)$ is the magnetic contribution (here ρ is the gas density and τ is the correlation time of the random flow). The latter is responsible for non-linear dynamo effects: $\alpha_{\rm m}$ and $\alpha_{\rm k}$ usually have opposite signs and, as $\overline{\boldsymbol{b} \cdot \boldsymbol{\nabla} \times \boldsymbol{b}}$ is amplified (together with or independently of $\overline{\boldsymbol{B}}$), the magnitude of the total α effect decreases, and this saturates the growth of the mean magnetic field.

The dynamo non-linearity resulting from the magnetic helicity conservation is governed by the following equation for the magnetic contribution to the α effect: (Kleeorin & Ruzmaikin 1982; Kleeorin et al. 1995; Subramanian & Brandenburg 2006) (see also Shukurov et al. 2006, for a form adapted to disc dynamos):

$$\frac{\partial \alpha_{\rm m}}{\partial t} = -\frac{2\eta_{\rm t}}{l^2 B_{\rm eq}^2} \boldsymbol{\mathcal{E}} \cdot \overline{\boldsymbol{B}} - \boldsymbol{\nabla} \cdot \boldsymbol{\mathcal{F}}, \qquad (2)$$

where l is the outer scale of the turbulence, $B_{\rm eq} = u\sqrt{4\pi\rho}$, with ρ the gas density, is the characteristic strength of magnetic field, here taken to correspond to energy equipartition with turbulence, $\boldsymbol{\mathcal{E}} = \overline{\boldsymbol{u} \times \boldsymbol{b}}$ is the mean turbulent electromotive force, and $\boldsymbol{\mathcal{F}}$ is a flux density of $\alpha_{\rm m}$ (related to the flux density of the small-scale magnetic helicity density). Ohmic dissipation has been neglected in equation (2), which is justified if the time scales considered are short compared to the resistive time scale (exceeding the galactic lifetime at galactic scales) or if the Ohmic diffusion is negligible compared to the helicity flux. In fact, the latter condition must hold in order to avert the catastrophic quenching of the dynamo. The flux density can be written as the sum of several contributions,

$$\boldsymbol{\mathcal{F}} = \boldsymbol{\mathcal{F}}_{\rm a} + \boldsymbol{\mathcal{F}}_{\rm d} + ...$$

where the advective flux density $\boldsymbol{\mathcal{F}}_{\rm a}$ and diffusive flux density $\boldsymbol{\mathcal{F}}_{\rm d}$ are the two that are considered in this work, although other contributions exist (Vishniac & Cho 2001; Ebrahimi & Bhattacharjee 2014), and, generally, can be stronger than the diffusive flux density (Vishniac & Shapovalov 2014).

The advective flux density is given by

$$\boldsymbol{\mathcal{F}}_{\rm a} = \overline{\boldsymbol{U}} \alpha_{\rm m}.$$

A vertical advective flux of $\alpha_{\rm m}$ is expected to be present because of galactic winds and fountain flow (Shukurov et al. 2006; Heald 2012; Bernet et al. 2013). The diffusive flux density (Kleeorin et al. 2002)

$$\boldsymbol{\mathcal{F}}_{\rm d} = -\kappa \boldsymbol{\nabla} \alpha_{\rm m},$$

has been detected in direct numerical simulations (Brandenburg et al. 2009), with $\kappa \approx 0.3\eta_{\rm t}$ as obtained from numerical simulations (Mitra et al. 2010).

The idea and equations of the dynamic non-linearity due to the magnetic helicity conservation were suggested in the early 1980s (Kleeorin & Ruzmaikin 1982). Nevertheless, for 10–20 more years, simple, heuristic prescriptions of the dependence of α on the mean magnetic field had been used widely until the essential role of the magnetic helicity balance in mean-field dynamos was fully appreciated in response to the discovery of effects of the fluctuation dynamo on the non-linear states of the mean-field dynamo (Vainshtein & Cattaneo 1992). Most popular was an algebraic form

$$\alpha = \frac{\alpha_{\rm k}}{1 + aB^2/B_{\rm eq}^2} \qquad (3)$$

where $B \equiv |\overline{\boldsymbol{B}}|$, known as an algebraic α-quenching prescription. Here a is a parameter of order unity which will be adjusted in Section 6.2 so as to achieve agreement with results obtained with the dynamical non-linearity (2). Until then, we assume $a = 1$, as is standard.

For the sake of simplicity, α and $\eta_{\rm t}$ are here assumed to be pseudoscalar and scalar (as appropriate in isotropic turbulence). In the approximation of the $\alpha\omega$-dynamo, the induction effects of the galactic differential rotation, which produces $\overline{B}_\phi$ from $\overline{B}_r$, are assumed to be stronger than the similar mean induction effects of the random flow. Then the relevant component of the α-tensor responsible for the generation of $\overline{B}_r$ from $\overline{B}_\phi$ is $\alpha_{\phi\phi}$.

3 GALACTIC DYNAMOS

In a thin disc, the kinetic contribution to the α-effect can be written as the product of r-dependent and z-dependent parts,

$$\alpha_{\rm k} = \alpha_0(r)\,\widetilde{\alpha}(z)\,, \tag{4}$$

where α_0 can be estimated as (Krause & Rädler 1980; Ruzmaikin et al. 1988; Brandenburg & Subramanian 2005),

$$\alpha_0 = \frac{l^2\Omega}{h}\,, \tag{5}$$

with h the disc half-thickness, a function of r in a flared disc, Ω the angular velocity of the gas, also a function of r, and l the correlation scale of the random velocity field. It follows from symmetry considerations that α is an odd function of z and $\alpha > 0$ for $z > 0$ (Ruzmaikin et al. 1988). As in numerous earlier analytical studies of the mean-field disc dynamos, we adopt

$$\widetilde{\alpha} = \sin\left(\frac{\pi z}{h}\right)\,.$$

The mean velocity in a disc galaxy is dominated by the azimuthal component, representing differential rotation, and the vertical (outflow) velocity, a wind or a fountain flow:

$$\overline{\boldsymbol{U}} = (0, r\Omega, \overline{U}_z)\,,$$

where $\overline{U}_z$ is the mass-weighted outflow speed. At small distances from the midplane, one can use

$$\overline{U}_z = U_0\widetilde{U}_z\,, \qquad \widetilde{U}_z = \frac{z}{h}\,. \tag{6}$$

We use the axisymmetric disc model of Chamandy et al. (2013a) that has a thin, stratified, differentially rotating, flared, turbulent disc with the turbulent scale and rms velocity of $l = 0.1\,$kpc and $u = 10\,{\rm km\,s^{-1}}$, and the mixing-length estimate of the turbulent magnetic diffusivity follows as

$$\eta_{\rm t} = \tfrac{1}{3}lu = 10^{26}\,{\rm cm^2\,s^{-1}}. \tag{7}$$

We also adopt $U_0 = 1\,{\rm km\,s^{-1}}$, constant with radius (Sur et al. 2007). For the galactic rotation curve, the Brandt's form

$$\Omega(r) = \frac{\Omega_0}{\left[1 + (r/r_\omega)^2\right]^{1/2}}\,,$$

with $r_\omega = 2\,$kpc, and $U_\phi = 250\,{\rm km\,s^{-1}\,kpc^{-1}}$ at $r = 10\,$kpc is chosen, resulting in $\Omega_0 \simeq 127\,{\rm km\,s^{-1}\,kpc^{-1}}$.

The disc half-thickness is assumed to vary hyperbolically with radius, $h(r) = h_{\rm D}\left[1 + (r/r_{\rm D})^2\right]^{1/2}$, where $h_{\rm D}$ is the scale height at $r = 0$, and $r_{\rm D} = 10\,$kpc controls the disc flaring rate. The value of h at $r = 10\,$kpc is chosen to be $0.5\,$kpc, which gives $h_{\rm D} \simeq 0.35\,$kpc. The equipartition magnetic field strength is taken as

$$B_{\rm eq} = B_0 \exp\left[-\frac{r}{R} - \frac{z^2}{2h^2}\right],$$

where $R = 20\,$kpc. This is equivalent to an exponential scale length of $10\,$kpc for the turbulent energy in the ionized gas. For comparison, this is similar to but slightly larger than the scale length $\sim 7\,$kpc of the total magnetic energy in the galaxy NGC 6946 (Beck 2007). The value of B_0 can be chosen as convenient, e.g. $B_0 = 8.2\,\mu$G to have $B_{\rm eq} \simeq 5\,\mu$G at $r = 10\,$kpc, $z = 0$.

We consider in detail specific models at $r = 4\,$kpc and $r = 8\,$kpc. It is convenient to define the dimensionless control parameters

$$R_\alpha \equiv \frac{\alpha_0 h}{\eta_{\rm t}}, \quad R_\omega \equiv \frac{Gh^2}{\eta_{\rm t}}, \quad R_U \equiv \frac{U_0 h}{\eta_{\rm t}}, \quad R_\kappa \equiv \frac{\kappa}{\eta_{\rm t}},$$

where $G = r\,\partial\Omega/\partial r$. Using equations (5) for α_0 and (7) for $\eta_{\rm t}$, the dynamo number is obtained as

$$D \equiv R_\alpha R_\omega = \frac{\alpha_0 G h^3}{\eta_{\rm t}^2} \simeq -9\frac{h^2\Omega^2}{u^2},$$

where the last equality applies to a flat rotation curve, $G = -\Omega$. Radially-dependent parameter values are given in Table 1.

4 BASIC EQUATIONS

We solve equations (1) and (2) in the thin-disc approximation ($h \ll r_\omega, r_{\rm D}, R$, hence $|B_z| \ll |B_r|, |B_\phi|$), where radial derivatives of $\overline{\boldsymbol{B}}$ are neglected, and assume $\eta_{\rm t} = $ const. In cylindrical coordinates, components of equations (1) and (2) become

$$\frac{\partial\overline{B}_r}{\partial t} = -\frac{\partial}{\partial z}\left(\alpha\overline{B}_\phi\right) + \eta_{\rm t}\frac{\partial^2\overline{B}_r}{\partial z^2} - \frac{\partial}{\partial z}\left(\overline{U}_z\overline{B}_r\right), \tag{8}$$

$$\frac{\partial\overline{B}_\phi}{\partial t} = G\overline{B}_r + \frac{\partial}{\partial z}\left(\alpha\overline{B}_r\right) + \eta_{\rm t}\frac{\partial^2\overline{B}_\phi}{\partial z^2} - \frac{\partial}{\partial z}\left(\overline{U}_z\overline{B}_\phi\right), \tag{9}$$

$$\frac{\partial\alpha_{\rm m}}{\partial t} = -\frac{2\eta_{\rm t}}{l^2 B_{\rm eq}^2}\left[\alpha\left(\overline{B}_r^2 + \overline{B}_\phi^2\right) - \eta_{\rm t}\left(\frac{\partial\overline{B}_r}{\partial z}\overline{B}_\phi - \frac{\partial\overline{B}_\phi}{\partial z}\overline{B}_r\right)\right] - \frac{\partial}{\partial z}\left(\overline{U}_z\alpha_{\rm m}\right) + \kappa\frac{\partial^2\alpha_{\rm m}}{\partial z^2}. \tag{10}$$

where we have neglected $\overline{B}_z\partial\overline{U}_\phi/\partial z$ in equation (9), and assumed $\overline{B}_z^2 \ll \overline{B}_r^2 + \overline{B}_\phi^2$ in equation (10). The solenoidality of $\overline{\boldsymbol{B}}$ implies that $\partial\overline{B}_z/\partial z \approx 0$ in a thin disc. Vacuum boundary conditions, $\overline{B}_r = \overline{B}_\phi = 0$ and $\partial^2\alpha_{\rm m}/\partial z^2 = 0$ at $z = \pm h$, are used. Under such conditions, the quadrupole mode, such that $\partial\overline{B}_r/\partial z = \partial\overline{B}_\phi/\partial z = \alpha_{\rm m} = 0$ at $z = 0$ emerges automatically. The boundary condition for $\alpha_{\rm m}$ leaves unconstrained the helicity flux through the disc surface.

4.1 Solutions of the disc dynamo equations

4.1.1 Dynamical non-linearity

Equations (8)–(10) are solved on a grid of 201 gridpoints in $-h \leqslant z \leqslant h$ using the 6th order finite differencing and 3rd order time-stepping schemes given in Brandenburg

Table 1. Key parameter values for the models studied. From left to right, the radius in the disc r, the disc scale height h, the vertical turbulent diffusion time $t_{\rm d} = h^2/\eta_{\rm t}$, the equipartition field strength $B_{\rm eq}$, the amplitude of the α effect α_0, the radial shear $G = rd\Omega/dr$, the amplitude of the outflow velocity U_0, and the turbulent diffusivity (of $\alpha_{\rm m}$) coefficient κ. This is followed by the dimensionless control parameters $R_\alpha \equiv \alpha_0 h/\eta_{\rm t}$, $R_\omega \equiv Gh^2/\eta_{\rm t}$, $R_U \equiv U_0 h/\eta_{\rm t}$, $R_\kappa \equiv \kappa/\eta_{\rm t}$ and $D \equiv R_\alpha R_\omega$. For the reader's convenience, both dimensionless and dimensional parameters are provided, e.g. R_U and U_0.

r [kpc]	h [pc]	$t_{\rm d}$ [Myr]	$B_{\rm eq}$ [B_0]	α_0 $\left[\frac{\rm km}{\rm s}\right]$	G $\left[\frac{\rm km}{\rm s\,kpc}\right]$	U_0 $\left[\frac{\rm km}{\rm s}\right]$	κ $\left[\frac{\rm km\,kpc}{\rm s}\right]$	R_α	R_ω	R_U	R_κ	D
4	381	425	0.82	1.50	−45.6	0/1	0/0.1	1.71	−19.8	0/1.14	0/0.3	−33.9
8	453	601	0.67	0.68	−29.1	0/1	0/0.1	0.93	−17.9	0/1.36	0/0.3	−16.6

(2003). The seed field is taken to be $\overline{B}_r = 10^{-3}B_0(1 - z^2/h^2)\exp(-z^2/h^2)$, $\overline{B}_\phi = 0$ at $t = 0$, and $\alpha_{\rm m} = 0$ initially. Solutions are not sensitive to the value or form of the seed field, as long as it is sufficiently weak.

4.1.2 Algebraic quenching

In the case of algebraic quenching, $\alpha_{\rm m}$ no longer enters the equations explicitly and equation (10) is not solved. Equations (8) and (9) are solved in the same manner as above but now with α replaced by expression (3), with $B^2 = \overline{B}_r^2 + \overline{B}_\phi^2$ and $a = 1$. Subsequently, equation (3) is refined using the no-z approximation to estimate a, and the simulations are repeated using this more accurate version of algebraic quenching.

4.1.3 Marginal kinematic solutions

If the action of the dynamical quenching is to ultimately diminish the value of α without drastically modifying its spatial variation, then it may be reasonable to simpy rescale α in the kinematic problem to a marginal value corresponding to $\partial/\partial t = 0$. Thus, equations (8) and (9) are solved with $\alpha = \alpha_{\rm k}$, as defined in equation (4). However, the right hand side of equation (5) is multiplied by a positive numerical factor < 1, which is varied iteratively until the growth rate of $\overline{\boldsymbol{B}}$ reduces to zero.

4.1.4 Perturbation solutions

It can be useful to have an analytic expression for $\overline{\boldsymbol{B}}$ in the kinematic regime, and such a solution has been derived using perturbation theory for the case $\overline{U}_z = 0$ (Shukurov 2007; Sur et al. 2007; Shukurov & Sokoloff 2008). This solution is extended to $\overline{U}_z \neq 0$ in Appendix A. For the exponential growth rate we obtain

$$\gamma = -\frac{\pi^2}{4} + \frac{\sqrt{-\pi D}}{2} - \frac{R_U}{2} + \frac{3\sqrt{-\pi D}R_U}{4\pi(\pi+4)} + \frac{R_U^2}{2\pi^2}\left(1 - \frac{\pi^2}{6}\right). \tag{11}$$

As in Section 4.1.3, the corresponding marginal solution is obtained by using the critical values for the dynamo number D and $R_\alpha = D/R_\omega$:

$$\overline{B}_r = C_0 R_{\alpha,{\rm c}}\left\{\cos\left(\frac{\pi z}{2}\right) + \frac{3}{4\pi^2}\left(\sqrt{-\pi D_{\rm c}} - \frac{R_U}{2}\right)\cos\left(\frac{3\pi z}{2}\right) + \frac{R_U}{2\pi^2}\sum_{n=2}^{\infty}\frac{(-1)^n(2n+1)}{n^2(n+1)^2}\cos\left[\left(n+\tfrac{1}{2}\right)\pi z\right]\right\}, \tag{12}$$

$$\overline{B}_\phi = -\frac{2}{\pi}C_0\sqrt{-\pi D_{\rm c}}\left\{\cos\left(\frac{\pi z}{2}\right) - \frac{3R_U}{8\pi^2}\cos\left(\frac{3\pi z}{2}\right) + \frac{R_U}{2\pi^2}\sum_{n=2}^{\infty}\frac{(-1)^n(2n+1)}{n^2(n+1)^2}\cos\left[\left(n+\tfrac{1}{2}\right)\pi z\right]\right\}, \tag{13}$$

where the subscript 'c' denotes critical values, $R_{\alpha,{\rm c}} = D_{\rm c}/R_\omega$, C_0 is a normalization constant that controls the steady-state strength of the magnetic field, and

$$D_{\rm c} = -\frac{\pi^3}{4}\left\{\frac{1 + 2R_U/\pi^2 - (2R_U^2/\pi^4)(1-\pi^2/6)}{1 + 3R_U/[2\pi(\pi+4)]}\right\}^2. \tag{14}$$

For practical purposes, it is sufficient to retain just a few terms in the infinite sums.

4.1.5 The no-z approximation

Finally, equations (8)–(10) can be solved in a steady state, $\partial/\partial t = 0$, in an approximate way as a set of algebraic equations using the no-z approximation (Subramanian & Mestel 1993; Moss 1995; Phillips 2001; Chamandy et al. 2013a) to replace z-derivatives by simple divisions by h, e.g. $\partial^2/\partial z^2 \sim -1/h^2$ and $\partial/\partial z \sim \pm 1/h$, with the sign chosen appropriately. This corresponds to using averages over the disc thickness. Using the fact that solutions have the form $B \propto {\rm e}^{\gamma t}$ in the kinematic regime, we also solve for the exponential growth rate γ. This leads to (see Appendix B for details):

$$D_{\rm c} = -\frac{\pi^5}{32}\left(1 + \frac{1}{\pi^2}R_U\right)^2, \tag{15}$$

$$\gamma = \frac{\pi^2}{4}t_{\rm d}^{-1}\left(1 + \frac{1}{\pi^2}R_U\right)\left(\sqrt{\frac{D}{D_{\rm c}}} - 1\right) = \sqrt{\frac{2}{\pi}}t_{\rm d}^{-1}\left(\sqrt{-D} - \sqrt{-D_{\rm c}}\right), \tag{16}$$

$$\tan p = -\left(\frac{2R_{\alpha,{\rm c}}}{\pi|R_\omega|}\right)^{1/2} = \frac{1}{4}\frac{R_U + \pi^2}{R_\omega}, \tag{17}$$

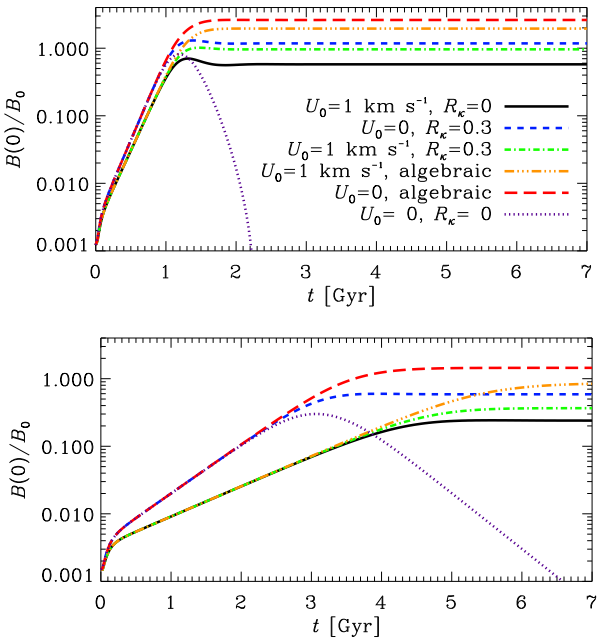

Figure 1. Evolution of the magnetic field strength at the midplane, normalized to the local equipartition field strength, for parameters corresponding to $r = 4\,\mathrm{kpc}$ (top) and $r = 8\,\mathrm{kpc}$ (bottom) in the disc model of Chamandy et al. (2013a). (See online version for colour figures.)

$$B^2 = B_{\rm eq}^2 \frac{\xi(p)}{C}\left(\frac{D}{D_{\rm c}} - 1\right)\left(R_U + \pi^2 R_\kappa\right), \qquad (18)$$

where $t_{\rm d} = h^2/\eta_{\rm t}$ is the turbulent diffusion time-scale, $p \equiv \arctan(\overline{B}_r/\overline{B}_\phi)$ is the magnetic pitch angle, $\xi(p) \equiv [1 - 3\cos^2 p/(4\sqrt{2})]^{-1}$ and $C \equiv 2(h/l)^2$. Note that γ decreases linearly with R_U in the no-z approximation.

5 RESULTS

5.1 Growth rate, temporal evolution and saturation

The time evolution of the magnetic field strength at the galactic midplane $z = 0$, normalized to the equipartition value $B_{\rm eq}$, is shown in Fig. 1, for parameters corresponding to $r = 4\,\mathrm{kpc}$ (top) and $r = 8\,\mathrm{kpc}$ (bottom). For solutions of the full set of equations (8)–(10) of Section 4.1.1, four different regimes are depicted, with and without the advective and diffusive helicity fluxes, $U_0 = 0$ or $1\,\mathrm{km\,s^{-1}}$ and $R_\kappa = 0$ or 0.3. Two cases with algebraic α quenching (Section 4.1.2) are also illustrated, with $U_0 = 0$ and $U_0 = 1\,\mathrm{km\,s^{-1}}$.

There is an initial brief phase of very rapid growth of the field at $z = 0$, but this reflects the arbitrary choice of the seed magnetic field and is not physically relevant. In all cases, the magnetic field then grows exponentially, until $B \sim B_{\rm eq}$. A steady state follows unless, in the dynamical quenching model, the flux of $\alpha_{\rm m}$ is zero ($R_\kappa = R_U = 0$), in which case the field decays catastrophically (dotted curves). The exponential growth rates γ in the kinematic regime are the same for all solutions with a given value of R_U, as would be expected. The growth rate of the magnetic field

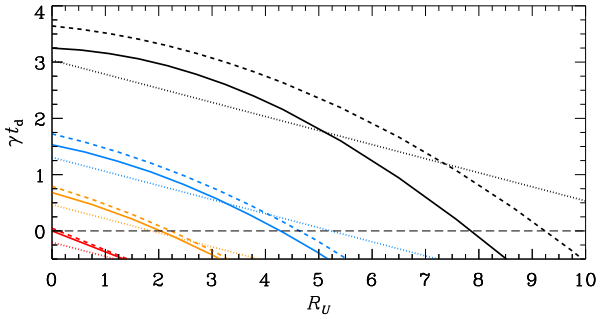

Figure 2. The dimensionless growth rate γ (measured in inverse diffusion time $t_{\rm d}^{-1}$) as a function of R_U for the numerical kinematic solutions (solid), the perturbation solution (short-dashed), and the no-z solution (dotted). Each color represents a different dynamo number/disc radius. From top to bottom: $D = -47.5$, $t_{\rm d} = 0.38\,\mathrm{Gyr}$ (black), $D = -22.4$, $t_{\rm d} = 0.50\,\mathrm{Gyr}$ (blue), $D = -13.5$, $t_{\rm d} = 0.73\,\mathrm{Gyr}$ (orange), and $D = -8.1$, $t_{\rm d} = 3.67\,\mathrm{Gyr}$ (red).

at $r = 4\,\mathrm{kpc}$ is larger than that at $r = 8\,\mathrm{kpc}$ since the dynamo number D is larger in magnitude at the smaller radius (Table 1). The growth rate at $r = 2\,\mathrm{kpc}$ (not shown here), where the eigenfunction for $\overline{\boldsymbol{B}}$ has a maximum in r in the model of Chamandy et al. (2013a), $\gamma = 8.5\,\mathrm{Gyr}^{-1}$ for $U_0 = 0$, is close (albeit slightly greater) to the global growth rate $\Gamma = 7.8\,\mathrm{Gyr}^{-1}$ in the axisymmetric global disc model of Chamandy et al. (2013a).

The growth rate in the numerical solutions can be compared with that obtained from the asymptotic solutions. Fig. 2 shows γ, in units of the inverse diffusion time $t_{\rm d}^{-1}$, plotted as a function of R_U, for various values of the dynamo number $-50 < D < -8$. Numerical solutions (solid) are well approximated by the perturbation solution (dashed), and the functional form $\gamma(R_U)$ is remarkably close to that of the numerical solution. The no-z solution gives values of γ that are somewhat less accurate (as might be expected) but still reasonable for growing solutions ($\gamma > 0$) unless D and R_U are both very large.

The steady-state field strength at the midplane, $B(0)$, increases with R_κ in the solutions with dynamical quenching (compare black solid and green dash-dotted curves of Fig. 1) since larger R_κ means larger diffusive helicity flux. Conversely, the saturation strength is smaller for larger R_U for the values of R_U considered (compare blue short dashed and green dash-dotted curves). The mean vertical velocity affects the dynamo action in more than one way. On the one hand, the steady-state magnetic field strength increases with R_U as in equation (18), but larger R_U means a larger magnitude of the critical dynamo number (15), hence a weaker dynamo action. As discussed by Sur et al. (2007), there exists a value of R_U optimal for the dynamo action. For $R_\kappa = 0.3$ and $r = 4\,\mathrm{kpc}$, the no-z approximation has the optimal value $R_U = 0.57$, while for $r = 8\,\mathrm{kpc}$ an outflow of any intensity reduces magnetic field strength in the steady state (formally, the optimum value is negative, $R_U = -0.68$). However, in the numerical solution with the dynamical quenching nonlinearity (that does not rely on the no-z approximation), $R_U = 0$ gives a higher saturation strength than any $R_U > 0$ at both $r = 4\,\mathrm{kpc}$ and $r = 8\,\mathrm{kpc}$ for $R_\kappa = 0.3$. Similar, but

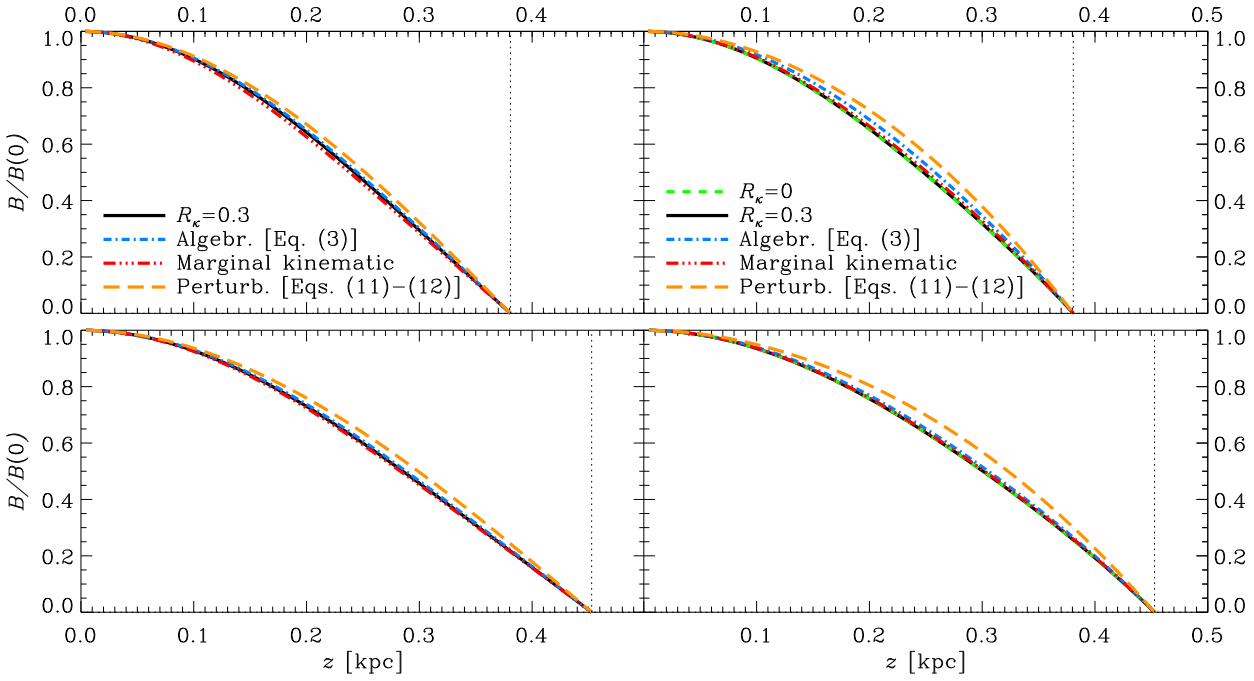

Figure 3. Dependence of the magnitude of the large-scale magnetic field B on height z. The upper panel is for $r = 4\,\mathrm{kpc}$ while the lower panel is for $r = 8\,\mathrm{kpc}$. Solutions with $U_0 = 0$ are shown on the left of each panel, while those with $U_0 = 1\,\mathrm{km\,s^{-1}}$ are shown on the right. The vertical dotted line shows the disk boundary at $z = h$. Solutions are symmetric about $z = 0$.

less transparent dependences on R_U can be noticed in the perturbation solution of Section 4.1.4. Similar dependence on R_U also occurs under the algebraic quenching (compare orange dash-triple-dotted and red long dashed curves), but here the mean vertical velocity can only be damaging for the dynamo action and the steady-state magnetic field decreases with R_U monotonically.

With the dynamical non-linearity, the field undergoes mild non-linear oscillations before settling down to a steady state (such oscillations are more evident for parameters corresponding to $r = 4\,\mathrm{kpc}$, but are present for $r = 8\,\mathrm{kpc}$ as well). Much milder oscillations are found for the case of algebraic quenching, for parameters corresponding to $r = 4\,\mathrm{kpc}$, but not at $r = 8\,\mathrm{kpc}$. This oscillatory behaviour is discussed by Sur et al. (2007) who attribute it to repeated over-suppression and recovery of the dynamo action by helicity fluxes.

It can be seen in both the top and bottom panels that for both $U_0 = 0$ and $U_0 = 1\,\mathrm{km\,s^{-1}}$, the saturated field strength obtained using algebraic quenching is higher than that obtained using dynamical quenching, by a factor of about 2–4. Since the algebraic quenching is of an entirely heuristic form, this difference is not of any physical significance. The agreement can thus be restored just by adjusting the factor a in equation (3); this is done in Section 6.

5.2 Magnetic field distribution across the disc

We now explore the dependence of B, $\overline{B}_r$, $\overline{B}_\phi$, p and α on the height z above the galactic midplane, in the saturated (steady) state. In Fig. 3, we plot B versus z for the various models, normalized to the value of B at $z = 0$ for each model, with $r = 4\,\mathrm{kpc}$ in the upper panel and $r = 8\,\mathrm{kpc}$ in the lower panel. On the left of each panel, $U_0 = 0$, whereas on the right, $U_0 = 1\,\mathrm{km\,s^{-1}}$. The profiles of $\overline{B}_r$ and $\overline{B}_\phi$, similarly normalized, are plotted in Fig. 4, while the magnetic pitch angle p is shown in Fig. 5 and the α profile in Fig. 6.

All of the curves lie strikingly close together. Clearly, the inclusion of a realistic outflow with $R_U \sim 1$ does not drastically affect the functional form of the solution, though some differences between solutions with $R_U = 0$ and $R_U > 0$ are apparent (see below). Furthermore, it is noteworthy that the difference between dynamical and algebraic quenching solutions is very small. The marginal kinematic and perturbation solutions (Sections 4.1.3 and 4.1.4, respectively) reproduce the functional forms of $\overline{B}_r$ and $\overline{B}_\phi$ quite accurately even though these are linear solutions. The agreement is equally good in the ratio $\overline{B}_r/\overline{B}_\phi$, so all of the models produce similar magnetic pitch angles $p \sim -10^\circ$ at $z = 0$ that reduces in magnitude with increasing distance from the midplane.

However, some small differences between the models do exist. As shown in Fig. 3, magnetic field strength B decreases with z slower as R_U increases (compare left and right plots in each panel). This is more evident for $r = 8\,\mathrm{kpc}$, where the difference between the solutions with $U_0 = 0$ and $U_0 = 1\,\mathrm{km\,s^{-1}}$ is already apparent at $z \gtrsim 0.15\,\mathrm{kpc}$. This is a natural consequence of the advection of magnetic field to regions with weaker field at larger z: such a redistribution is opposed by magnetic diffusion, and R_U is a measure of the strength of advection relative to diffusion (see also Bardou et al. 2001, who include a halo in their models).

The ratio $\overline{B}_r/\overline{B}_\phi$ of the magnetic field components shown in Fig. 4 is larger in magnitude near $z = 0$ when

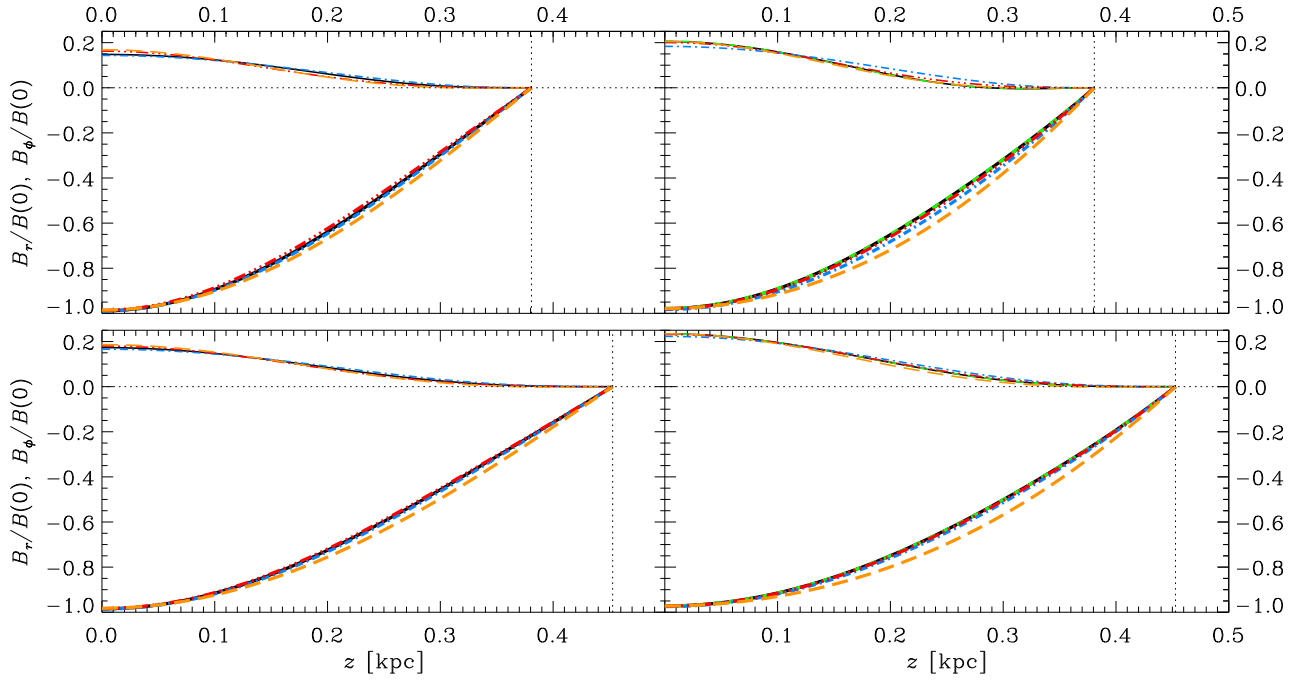

Figure 4. Radial (thin) and azimuthal (thick) components of $\overline{\boldsymbol{B}}$ in the saturated state, normalized to the magnetic field strength at the midplane for parameters corresponding to $r = 4\,\mathrm{kpc}$ (top) and $r = 8\,\mathrm{kpc}$ (bottom) and to $U_0 = 0$ (left) and $U_0 = 1\,\mathrm{km\,s^{-1}}$ (right). The sign of each component is arbitrary (see text), but the sign of $\overline{B}_r\overline{B}_\phi$ is not. Solutions are symmetric about $z = 0$. (For the legend, see Fig. 3.)

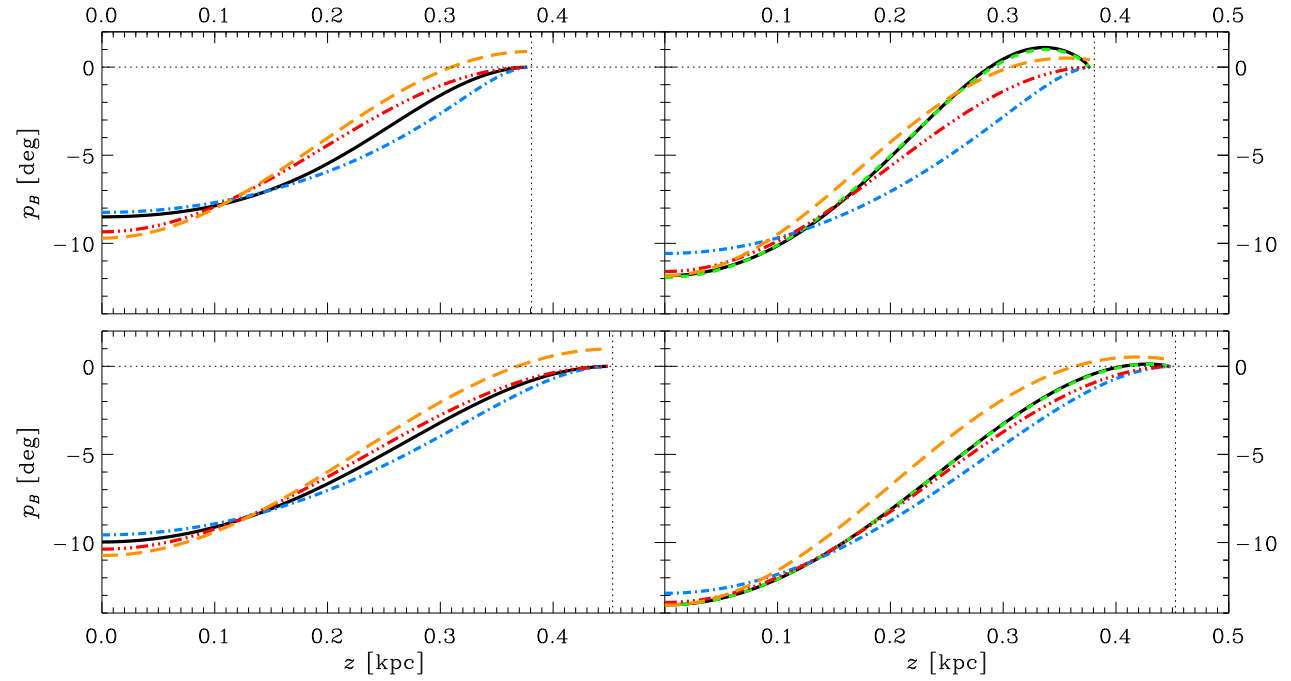

Figure 5. Magnetic pitch angle $p \equiv \tan^{-1}(\overline{B}_r/\overline{B}_\phi)$ in the saturated (steady) state, as a function of the distance z from the midplane, for parameters corresponding to $r = 4\,\mathrm{kpc}$ (top) and $r = 8\,\mathrm{kpc}$ (bottom) and to $U_0 = 0$ (left) and $U_0 = 1\,\mathrm{km\,s^{-1}}$ (right). p is not plotted for $z = h$, as it is undefined at the disc boundaries, where the boundary conditions enforce $\overline{B}_r = \overline{B}_\phi = 0$. (For the legend, see Fig. 3.)

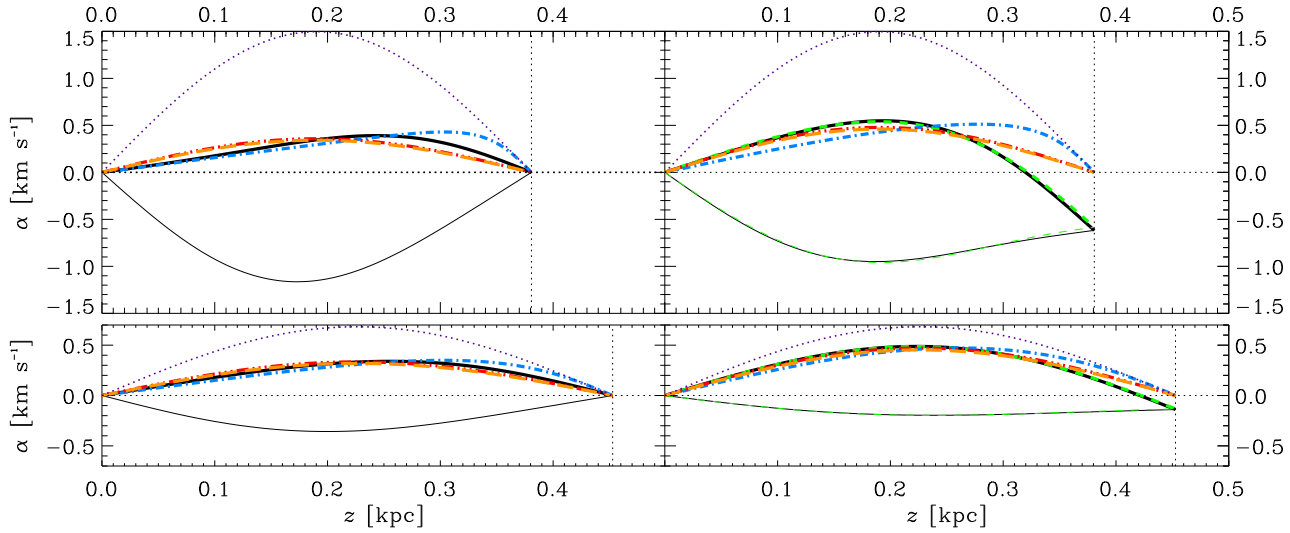

Figure 6. α in the saturated state as a function of the distance z from the midplane, for parameters corresponding to $r = 4\,\mathrm{kpc}$ (top) and $r = 8\,\mathrm{kpc}$ (bottom) and to $U_0 = 0$ (left) and $U_0 = 1\,\mathrm{km\,s^{-1}}$ (right). For the asymptotic solution, α has been plotted as $(\pi R_{\alpha,\mathrm{c}}\eta_\mathrm{t}/2h)\sin(\pi z/h)$. α_k is shown as a thin dotted purple line for comparison. For solutions using the dynamical quenching nonlinearity, α_m is shown as a thin line of the appropriate linestyle. All functions shown are antisymmetric about $z = 0$. (For the legend, see Fig. 3.)

Table 2. Comparison of the results of the numerical solution of Section 4.1.1 and the no-z solution of Section 4.1.5. For the numerical solution, vertical averages of p and B/B_eq, defined in equations (19), are given.

			Numerical solution				No-z approximation			
r [kpc]	R_U	R_κ	D_c	γ [Gyr^{-1}]	$\langle p\rangle$ [°]	$\langle B\rangle/B_\mathrm{eq}$	D_c	γ [Gyr^{-1}]	p [°]	B/B_eq
4	0.0	0.3	− 8.1	5.6	−6.6	0.79	− 9.6	5.1	−7.1	0.74
	1.1	0.0	−10.8	5.2	−7.7	0.40	−11.9	4.5	−7.9	0.39
	1.1	0.3	−10.8	5.2	−7.7	0.66	−11.9	4.5	−7.9	0.74
8	0.0	0.3	− 8.1	1.7	−7.2	0.39	− 9.6	1.3	−7.9	0.33
	1.4	0.0	−11.5	1.0	−9.1	0.17	−12.4	0.7	−8.9	0.15
	1.4	0.3	−11.5	1.0	−9.1	0.26	−12.4	0.7	−8.9	0.27

$R_U \neq 0$, and the ratio is larger when R_U is larger. This can be seen more clearly in Fig. 5, which shows the magnetic pitch angle p as a function of z. The increase of $|p|$ with R_U is a direct consequence of equation (17).

A notable feature of models with $R_U > 0$ is that the magnetic pitch angle changes sign near the disc surface, so that a trailing (with respect to the overall rotation) magnetic spiral of the inner layers becomes a leading spiral near the disc surface. This is a characteristic feature of any growing dynamo mode in a slab surrounded by vacuum (Ruzmaikin et al. 1979; Ji et al. 2013), but not of a marginal kinematic solution where $p < 0$ everywhere in the slab. The outflow extends this feature to the steady state. The reversal of $\overline{B}_r$ responsible for this occurs deeper in the slab as the dynamo number is increased. Thus, a leading, rather than a trailing, magnetic spiral may exist in the disc near the disc-halo boundary (and perhaps in the halo), provided that an outflow is present. However, the robustness of this feature should be checked using other types of boundary condition which may be more suitable for outflows, or by including the galactic halo in the model.

The perturbation solution of Section 4.1.4 also has $p > 0$ near the surface for both vanishing and positive R_U. This is an artefact resulting from the loss of accuracy of this solution which is formally applicable only for $|D| \ll 1$ and $R_U \ll 1$. As discussed by Ji et al. (2013), the solution remains accurate even for $D \simeq -50$, but this is, evidently, not the case with R_U. Hence, the perturbation solution should not be used for R_U of order unity if the behaviour of the solution near the surface is important.

The change in the sign of α near the boundaries can be understood as resulting from the advective flux of α_m towards the boundaries. Since the kinetic part of the α-coefficient is small near $z = h$, advection of the (negative) α_m from deeper layers can change the sign of $\alpha = \alpha_\mathrm{k} + \alpha_\mathrm{m}$ near the surface. The effect is more pronounced at smaller radius because α_m has larger magnitude there (see Fig. 6 where α_m is shown as a thin line of the appropriate linestyle and color). It would be useful to explore how sensitive is this effect to the boundary conditions.

6 THE ALGEBRAIC NON-LINEARITY AND NO-z APPROXIMATION REFINED

Both the no-z approximation and the algebraic form of the dynamo non-linearity are simple, convenient and flexible approaches, and we have demonstrated that they approximate quite reasonably the physically motivated dynamo solutions with dynamic non-linearity. Then they deserve to be refined to achieve better quantitative agreement with the results obtained under the dynamic non-linearity.

6.1 Improved no-z approximation

Numerical solutions of equations (8)–(10) are compared with those obtained with the no-z approximation in Table 2. Since the latter can be thought of as representing equivalent (averaged over the disc thickness) values of the solution, we present, for the numerical solutions, the averaged magnetic field strength and pitch angle defined as

$$\langle\overline{B}\rangle = \frac{1}{2h}\int_{-h}^{h}\overline{B}\,\mathrm{d}z\,, \quad \tan\langle p\rangle = \frac{\displaystyle\int_{-h}^{h}\frac{\overline{B}_r}{\overline{B}_\phi}\,\overline{B}\,\mathrm{d}z}{\displaystyle\int_{-h}^{h}\overline{B}\,\mathrm{d}z}\,. \qquad (19)$$

We note that these averages may differ from those obtained from observations of polarized intensity or Faraday rotation where the observables are the Stokes parameters that depend on higher powers of magnetic field.

In addition to the terms used in the earlier applications of the no-z approximation, we have additional terms representing magnetic helicity fluxes. Magnetic field components in equations (12) and (13) depend on z in a more complicated manner if $R_U \neq 0$. This suggests that approximating derivatives in z with division by h would be less accurate and general when $R_U \neq 0$. Adjustments required to approximate the kinematic growth rate of the mean magnetic field with a reasonable accuracy for $-50 < D < 0$ are discussed in Appendix B1. We suggest and use the following approximations:

$$\frac{\partial}{\partial z}(\overline{U}_z\overline{B}_r) \simeq \frac{\overline{U}_z\overline{B}_r}{4h}\,, \qquad \frac{\partial}{\partial z}(\overline{U}_z\overline{B}_\phi) \simeq \frac{\overline{U}_z\overline{B}_\phi}{4h}\,,$$
$$\frac{\partial}{\partial z}(\overline{U}_z\alpha_\mathrm{m}) \simeq \frac{\overline{U}_z\alpha_\mathrm{m}}{h}\,, \qquad \frac{\partial^2\alpha_\mathrm{m}}{\partial z^2} \simeq -\pi^2\frac{\alpha_\mathrm{m}}{h^2}\,.$$

6.2 Algebraic α-quenching as an approximation to the dynamic non-linearity

The algebraic α-quenching appears to be a reasonable approximation to the dynamic non-linearity arising from magnetic helicity fluxes. We show in this section that this is not a coincidence by deriving an algebraic approximation to the dynamic non-linearity in the steady state, which contains terms responsible for the helicity transport, and discuss conditions for the applicability of this approximation.

To explore the steady state solution, set $\partial\alpha_\mathrm{m}/\partial t = 0$ in equation (2), generalized to include the Ohmic term (Sur et al. 2007). Assuming that the flux term can be approximated as $l^2\boldsymbol{\nabla}\cdot\boldsymbol{\mathcal{F}}/(2\eta_\mathrm{t}) = f\alpha_\mathrm{m}$, where f is a positive numerical factor to be determined, and putting $\alpha_\mathrm{m} = \alpha - \alpha_\mathrm{k}$, we obtain

$$\alpha = \alpha_\mathrm{c} = \frac{\alpha_\mathrm{k} + (f + 1/\mathcal{R}_\mathrm{m})^{-1}\,\eta_\mathrm{t}\boldsymbol{\nabla}\times\overline{\boldsymbol{B}}\cdot\overline{\boldsymbol{B}}}{1 + (f + 1/\mathcal{R}_\mathrm{m})^{-1}\,B^2}. \qquad (20)$$

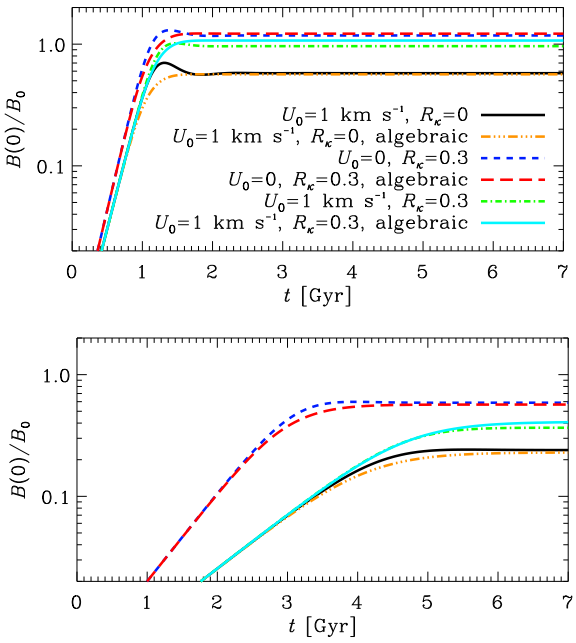

Figure 7. Time evolution of the magnetic field strength at $z = 0$ for models using dynamical quenching and models with the same parameters but using generalized algebraic quenching with a given by equation (23). Parameters corresponding to $r = 4\,\mathrm{kpc}$ are plotted in the top panel, and to $r = 8\,\mathrm{kpc}$ in the bottom panel.

where α_c is the critical value of α and the magnetic Reynolds number is here defined as $R_\mathrm{m} \equiv \eta_\mathrm{t}/\eta$. For $f = 0$ (no flux of α_m), this reduces to equation (14) of Gruzinov & Diamond (1994).

The algebraic form (3) follows from equation (20) if

$$\eta_\mathrm{t}\boldsymbol{\nabla}\times\overline{\boldsymbol{B}}\cdot\overline{\boldsymbol{B}} = K\alpha_\mathrm{c}B^2, \qquad (21)$$

with K a factor to be determined. Magnetic helicity balance constrains K to be positive, since α_c has opposite sign to α_m, and large- and small-scale current helicities must have opposite sign to each other.

Equation (21) is satisfied reasonably well for typical galactic parameters. Combining equations (B2) and (17) of the no-z solution, recalling that $D_\mathrm{c} = h\alpha_\mathrm{c}R_\omega/\eta_\mathrm{t}$, and assuming $\overline{B}_r^2/\overline{B}_\phi^2 \ll 1$, typical of $\alpha\omega$-dynamos, we obtain

$$K = \frac{3}{4\sqrt{2}} \approx 0.53. \qquad (22)$$

Furthermore, substituting $\alpha_\mathrm{k}/\alpha_\mathrm{c}$ for D/D_c in equation (18), and solving for α_c (assuming $\overline{B}_r^2/\overline{B}_\phi^2 \ll 1$), we obtain the form (3) with

$$a = \frac{C}{\xi_0(R_U + \pi^2 R_\kappa)}\,, \qquad (23)$$

where $\xi_0 = [1 - 3/(4\sqrt{2})]^{-1} \approx 2.1$ and $C \equiv 2(h/l)^2$, and the numerical factors in the no-z approximation estimated in Section 6.1 have been used in the helicity flux terms. This result can also be obtained from equations (20), (21), and (22), with $f = (R_U + \pi^2 R_\kappa)/C$. Specific values of a at $r = 4\,\mathrm{kpc}$ and $r = 8\,\mathrm{kpc}$ in the galaxy model adopted range

from 3–14 for the combinations of parameter values listed in Table 2. Note that this is consistent with the saturation value of B being a factor of about 2–4 too large (compared to that obtained with the dynamical non-linearity) when using algebraic quenching with $a = 1$, as noted in Section 5.1. Also note that these values for a are somewhat sensitive to the ratio h/l appearing in equation (23). Gressel et al. (2013) find even larger values of a from direct numerical simulations.

Equation (23) appears as a natural generalization of the standard α-quenching, as it makes the saturation magnetic field dependent on the magnetic helicity fluxes. Figure 7 compares the results obtained numerically with (3) and (23) with those under dynamical quenching. Clearly, the agreement is much better than for $a = 1$ (see Fig. 1). The z-distributions of the resulting magnetic field components are identical to those under the standard algebraic quenching with $a = 1$.

7 EXAMPLES OF APPLICATION

To illustrate the use of the toolbox, we apply it to estimate the magnetic pitch angle and to explore the nature of the magnetic arms. The analysis below is mainly based on the analytical expressions of the no-z approximation, but results have been checked with numerical solutions.

7.1 Magnetic pitch angle

In the kinematic stage, the pitch angle of the mean magnetic field, $p = \arctan(\overline{B}_r/\overline{B}_\phi) \simeq -\arctan(R_\alpha/|R_\omega|)^{1/2}$, agrees reasonably well with observations, even if its magnitude remains somewhat smaller than desired (Ruzmaikin et al. 1988). Some galaxies with exceptionally open magnetic spirals with $p \simeq -40^\circ$, such as M33 (Tabatabaei et al. 2008; Chyży & Buta 2008), do not seem to be consistent with this estimate.

Non-linear dynamo effects can only reduce the magnitude of the pitch angle since, effectively, they lead to the reduction of R_α to the smaller $R_{\alpha,\mathrm{c}}$ (see also Elstner 2005). Indeed, for the fairly typical galactic parameters chosen in the present work, we obtain $p \sim -10^\circ$ in the non-linear solutions, whereas average observed values are closer to -20° (Fletcher 2010; see also the discussion in Chamandy et al. 2014).

According to equation (17), $|p|$ increases with R_U, but increasing R_U also causes γ and B^2 to decrease, according to equations (16) and (18), and there is a maximum value of R_U above which the dynamo action is suppressed. From equation (15), the dynamo remains active for $R_U + \pi^2 < 4\sqrt{(2/\pi)\,R_\alpha|R_\omega|}$, which leads to a lower limit on the magnetic pitch angle:

$$\tan p > -\sqrt{\frac{2R_\alpha}{\pi|R_\omega|}}\,,$$

so that the outflow can hardly enhance the magnitude of p significantly. The right-hand side of the equation is simply the estimate one obtains for the kinematic regime; for the dynamical non-linearity that is assumed, $R_{\alpha,\mathrm{c}} < R_\alpha$, so $|p|$ always decreases from its value in the kinematic regime.

It appears that magnetic pitch angle of the dynamo-generated magnetic field is further modified by additional effects, some of which are rather obvious. Most importantly, magnetic field compression in the gaseous spiral arms efficiently aligns magnetic field with the spiral arms. If the ratio of the gas densities in the arm and outside it is ϵ, with $\epsilon > 1$ and $\epsilon = 4$ for a strong adiabatic shock, the angle θ between magnetic field and the arm axis is reduced, under one-dimensional compression, as $\tan\theta_2 = \epsilon^{-1}\tan\theta_1$ from the interarm value θ_1 to that within the arm θ_2. For $\theta_1 = 30^\circ$ and $\epsilon = 4$, magnetic field is diverted by $\theta_1 - \theta_2 \approx 22^\circ$ towards the arm axis. Since such observables as the Faraday rotation measure and polarized synchrotron intensity are dominated by the denser and stronger magnetized interior of the spiral arms, the compressional alignment can significantly affect the magnetic pitch angle observed.

Additional dynamo effects can also make the magnetic spirals more open. For example, the contribution of magnetic buoyancy to the mean-field dynamo action can produce $p = -(20^\circ$–$30^\circ)$ (Moss et al. 1999). Another, less obvious effect can be due to a radial inflow of interstellar gas (at a speed of order $U_r = 1\,\mathrm{km\,s^{-1}}$ at the Solar radius in the Milky Way, and expected to be stronger in galaxies with more open spiral patterns), driven by the outward angular momentum transfer by the spiral pattern, turbulence and magnetic fields. The inflow can increase the magnitude of p by at least 5–10%. (Moss et al. 2000). The effect of the many further additional terms in the mean electromotive force (e.g. Rohde et al. 1999; Rädler et al. 2003; Brandenburg & Subramanian 2005) on the pitch angle has never been explored.

7.2 Arm-interarm contrast in magnetic field strength

Various solutions of the dynamo equations offer a range of possibilities to explore the effects of spiral arms on the large-scale galactic magnetic fields. Among them are the phenomenon of magnetic arms, the enhancement of polarized intensity (and, presumably, the large-scale magnetic field) in spiral-shaped regions that do not always overlap with the gaseous arms, regions of larger gas density (e.g., Frick et al. 2000). Several explanations have been suggested (Moss 1998; Shukurov 1998; Rohde et al. 1999; Chamandy et al. 2013a,b; Moss et al. 2013), but there is no convincing explanation.

Equation (18) suggests a number of effects that can contribute to a non-monotonic dependence of the large-scale magnetic field strength on gas density. One possibility is that R_U can be larger in the arms owing to a greater frequency of supernova explosions there. This can lead to larger B^2/B_{eq}^2 in the interarm regions compared to in the arms, as suggested by Sur et al. (2007). An estimate of this effect can be found in Table 2: for $r = 8\,\mathrm{kpc}$ $\overline{B}$ would be about 1.5 times stronger in the interarm regions in an extreme case where the outflow speed vanishes between the arms remaining modest in the arms at $1\,\mathrm{km\,s^{-1}}$ ($R_U = 1.36$). This ratio increases to about 4 if $U_0 = 2\,\mathrm{km\,s^{-1}}$ in the arms. Therefore, this effect may be important and thus deserves a more detailed exploration.

8 CONCLUSIONS AND DISCUSSION

We have discussed various simple approximate approaches to estimate the strength of the large-scale galactic magnetic fields, their pitch angle and dynamo thresholds, and compared them with numerical solutions. In particular, we compared the non-linear states established due to magnetic helicity conservation with those obtained with a much simpler, and easier to analyze, heuristic algebraic form of the dynamo non-linearity. These approaches complement one another. For example the perturbation solution of Section 4.1.4 provides a reasonably accurate form of the distribution of magnetic field across the disc, whereas the no-z approximation of Section 4.1.5 gives useful results for variables averaged across the disc. Remarkably, and reassuringly, where they overlap, all of these methods result in similar solutions. Most importantly, results obtained with the dynamical non-linearity that involves advective and diffusive fluxes of magnetic helicity are very much consistent with those from the algebraic α-quenching. We suggest how the latter can be modified to achieve quite a detailed agreement.

Magnetic lines produced by the mean-field dynamo are believed to be trailing with respect to the galactic rotation because the galactic angular velocity decreases with galactocentric radius. We have found, however, that steady-state magnetic fields obtained for the dynamical non-linearity are trailing near the galactic midplane but leading closer to the disc surface (where $\overline{B}_r$ changes sign) if an outflow is present. This effect is more pronounced when the galactic outflow is stronger or the dynamo number is higher as compared with its critical value. This feature is new and unexpected, as it is not reproduced in models with algebraic quenching. This makes it reasonable to expect that leading magnetic spirals may be observable in the disc-halo interface regions of spiral galaxies (or even higher in the halo). To what extent this feature persists if the boundary conditions are varied or if the galactic halo is included is a question that merits future investigation.

It is also useful for applications that marginal kinematic solutions of the dynamo equations in a thin disc (i.e., those that neither grow nor decay) reproduce with high accuracy non-linear steady-state solutions. The simple analytical perturbation solutions of kinematic dynamo equations, here generalized to include magnetic field advection in a galactic outflow, are particularly useful in this respect. It has been shown here and by Ji et al. (2013) that they remain accurate beyond their formal range of applicability and can be used for the range of dynamo numbers $-50 \lesssim D \lesssim 0$ typical of galactic discs. Here we have also shown that these solutions can be used as a good approximation to the non-linear states.

We have also refined the no-z approximation to allow for vertical advection of the mean magnetic field, as well as advective and diffusive helicity fluxes. We note that advection affects dynamo action through three channels: by reducing the critical dynamo number, by helping the turbulent diffusion to remove flux from the dynamo active region, and by the removal of small-scale magnetic helicity. The heuristic diffusive flux of magnetic helicity has previously been observed in numerical simulations.

The models investigated here are somewhat simplified compared to real galaxies. It is worth extending the models to include spatial variation of $\eta_{\rm t}$, additional terms in the mean electromotive force, and other contributions to the magnetic helicity flux. The possible importance of $\eta_{\rm t}$-quenching, in addition to α-quenching (Gressel et al. 2013), also deserves exploration. More refined modelling will enable better comparison with real galaxies.

In summary, much of the earlier work on galactic dynamos modeled the saturation of the dynamo using algebraic quenching of the α effect. We show here that this algebraic quenching non-linearity (which predates dynamical quenching theory but is still widely used in the dynamo literature) is a good approximation to dynamical quenching for the galactic mean-field dynamo. We also extend the standard algebraic quenching formula to make it more accurate. In addition, we suggest three simple tools, namely marginal kinematic solutions, critical asymptotic solutions from perturbation theory, and no-z solutions, and show that all agree remarkably well with the numerical solutions of the non-linear dynamo. Particularly useful are the analytical expressions (12) and (13) for the vertical profiles of $\overline{B}_r$ and $\overline{B}_\phi$, as well as equations (18) and (17) for the saturation field strength B and pitch angle p, which, when used along with the analytical expression (11) for the kinematic growth rate γ, comprise a surprisingly efficient guide to the parameter space of galactic dynamos.

ACKNOWLEDGMENTS

We are grateful to Fred Gent and Aritra Basu for useful discussions, and to Nishant Singh for critical reading of an earlier version of the manuscript. AS acknowledges financial support of STFC (grant ST/L005549/1) and the Leverhulme Trust (grant RPG-097), and expresses his gratitude to IUCAA for hospitality and financial support.

APPENDIX A: PERTURBATION SOLUTIONS OF THE DYNAMO EQUATIONS WITH AN OUTFLOW

The kinematic $\alpha\Omega$ dynamo in a thin disc is governed by equation (8) and equation (9) with the α term omitted in equation (9). These can be written in dimensionless form as (e.g. Shukurov 2007):

$$\frac{\partial \overline{B}_r}{\partial t} = -R_\alpha \frac{\partial}{\partial z}(\widetilde{\alpha}\overline{B}_\phi) + \frac{\partial^2 \overline{B}_r}{\partial z^2} - R_U \frac{\partial}{\partial z}(\widetilde{U}_z \overline{B}_r), \quad \text{(A1)}$$

$$\frac{\partial \overline{B}_\phi}{\partial t} = R_\omega \overline{B}_r + \frac{\partial^2 \overline{B}_\phi}{\partial z^2} - R_U \frac{\partial}{\partial z}(\widetilde{U}_z \overline{B}_\phi), \quad \text{(A2)}$$

with the vacuum boundary conditions at the disc surface,

$$\overline{B}_r|_{z=\pm 1} = \overline{B}_\phi|_{z=\pm 1} = 0,$$

and where $\overline{B}_z$ can be recovered from the solenoidality condition. We make the equations time-independent by substituting the solution $\overline{\boldsymbol{B}} = \boldsymbol{\mathcal{B}}(z)\mathrm{e}^{\gamma t}$, and make the transformation

$$\mathcal{B}'_r \equiv R_\alpha^{-1}\mathcal{B}_r, \quad \mathcal{B}'_\phi \equiv \mathcal{B}_\phi/\sqrt{|D|}, \quad \text{(A3)}$$

where $D \equiv R_\omega R_\alpha$, and then drop primes for presentational convenience, so that equations (A1) and (A2) become

$$\gamma \mathcal{B}_r = -\sqrt{|D|}\frac{d}{dz}(\widetilde{\alpha}\mathcal{B}_\phi) + \frac{d^2\mathcal{B}_r}{dz^2} - R_U\frac{d}{dz}(\widetilde{U}_z\mathcal{B}_r),$$

$$\gamma \mathcal{B}_\phi = \sqrt{|D|}\mathrm{sign}(D)\mathcal{B}_r + \frac{d^2\mathcal{B}_\phi}{dz^2} - R_U\frac{d}{dz}(\widetilde{U}_z\mathcal{B}_\phi).$$

We then seek an asymptotic solution to this eigenvalue problem by treating terms involving $\sqrt{|D|}$ and R_U as a perturbation to the eigensolutions of the 'free-decay' modes ($D = R_U = 0$) of the diffusion equation. This generalizes the treatment of Shukurov (2007); Sur et al. (2007); Shukurov & Sokoloff (2008), who solve the case $R_U = 0$. We may write

$$(\widehat{W} + \epsilon\widehat{V})\boldsymbol{\mathcal{B}} = \gamma\boldsymbol{\mathcal{B}}, \tag{A4}$$

where $\epsilon = \mathrm{const}$ is a mathematical device to keep track of the orders, and is taken to be $\ll 1$ for the perturbation analysis before being 'restored' to its true value of unity at the end of the calculation (e.g. Griffiths 2005). The unperturbed operator $\widehat{W}$ is given by

$$\widehat{W} = \begin{pmatrix} \dfrac{d^2}{dz^2} & 0 \\ 0 & \dfrac{d^2}{dz^2} \end{pmatrix},$$

while the perturbation operator $\widehat{V}$ is given by

$$\widehat{V} = \begin{pmatrix} -R_U\dfrac{d}{dz}(z\cdots) & -\sqrt{-D}\dfrac{d}{dz}\left[\sin(\pi z)\cdots\right] \\ -\sqrt{-D} & -R_U\dfrac{d}{dz}(z\cdots) \end{pmatrix},$$

where we have adopted the forms (5) and (6) for $\widetilde{\alpha}$ and $\widetilde{U}_z$, and taken $\mathrm{sign}(D) = -1$, as is suitable for the present context.

Keeping terms containing both $\sqrt{-D}$ and R_U, we effectively assume that they are of the same order of magnitude. However, Ji et al. (2013) show that the resulting perturbation solution remains accurate up to $\sqrt{-D} \gtrsim 1$ (they consider the case $R_U = 0$). Then the requirement that $\sqrt{-D} = \mathcal{O}(R_U)$ is rather formal and not restrictive for practical purposes.

The eigensolutions of the unperturbed system $\widehat{W}\boldsymbol{b}_n = \lambda_n\boldsymbol{b}_n$ (with the above boundary conditions) are doubly degenerate and given by

$$\lambda_n = -\left(n + \tfrac{1}{2}\right)^2\pi^2, \quad n = 0, 1, 2, \ldots,$$

$$\boldsymbol{b}_n = \begin{pmatrix} \sqrt{2}\cos[(n+\frac{1}{2})\pi z] \\ 0 \end{pmatrix},$$

$$\boldsymbol{b}'_n = \begin{pmatrix} 0 \\ \sqrt{2}\cos[(n+\frac{1}{2})\pi z] \end{pmatrix},$$

where eigenfunctions have been normalized to $\int_0^1 \boldsymbol{b}_n^2 dz = \int_0^1 \boldsymbol{b}'^2_n dz = 1$ (the eigenfunctions should not be confused with the small-scale magnetic field, denoted $\boldsymbol{b}$ in the main text).

The expansions

$$\gamma = \gamma_0 + \epsilon\gamma_1 + \epsilon^2\gamma_2 + \ldots,$$

$$\boldsymbol{\mathcal{B}} = C_0\boldsymbol{b}_0 + C'_0\boldsymbol{b}'_0 + \epsilon\sum_{n=1}^{\infty}(C_n\boldsymbol{b}_n + C'_n\boldsymbol{b}'_n) + \ldots$$

are substituted into equation (A4), terms of like order in ϵ collected, the dot product of the resulting equations taken first with $\boldsymbol{b}_n$ and then with $\boldsymbol{b}'_n$, and the results integrated over $0 \leqslant z \leqslant 1$. [Note that the lowest order contribution to the eigenfunction can be assumed to be a linear combination of the fastest growing ($n = 0$) terms only.] To the lowest order this yields $\gamma_0 = \lambda_0$. A homogeneous system of algebraic equations for C_0 and C'_0 follows from terms of order ϵ, whose solvability condition yields

$$\gamma_1 = \frac{1}{2}\left\{(V_{00} + V_{0'0'}) + \left[(V_{00} - V_{0'0'})^2 + 4V_{00'}V_{0'0}\right]^{1/2}\right\}$$
$$= -\frac{R_U}{2} + \frac{\sqrt{-\pi D}}{2},$$

and

$$C'_0 = \frac{(\gamma_1 - V_{00})}{V_{00'}}C_0 = -\frac{2}{\sqrt{\pi}}C_0,$$

where we have retained only the root corresponding to the growing solution. Here $V_{nm} \equiv \int_0^1 \boldsymbol{b}_n \cdot \widehat{V}\boldsymbol{b}_m dz$ are the perturbation matrix elements, whose direct calculation yields

$$V_{00'} = -\pi\sqrt{-D}/4, \quad V_{0'0} = -\sqrt{-D},$$
$$V_{00} = V_{0'0'} = -\frac{R_U}{2}.$$

The eigenvalue can be evaluated to a higher order in ϵ than the eigenfunction since it depends on the matrix elements $V_{\tilde{0}n}$, $V_{\tilde{0}n'}$, $V_{n\tilde{0}}$, and $V_{n'\tilde{0}}$, where, e.g., $V_{\tilde{0}n} \equiv \int_0^1 \tilde{\boldsymbol{b}}_0 \cdot \widehat{V}\boldsymbol{b}_n dz$, and

$$\tilde{\boldsymbol{b}} \equiv C_0\boldsymbol{b}_0 + C'_0\boldsymbol{b}'_0 = C_0\begin{pmatrix} 1 \\ -2/\sqrt{\pi} \end{pmatrix}\sqrt{2}\cos\left(\frac{\pi z}{2}\right).$$

The above method then yields:

$$\gamma_2 = \sum_{n=1}^{\infty}\frac{V_{n\tilde{0}}V_{\tilde{0}n} + V_{n'\tilde{0}}V_{\tilde{0}n'}}{\lambda_0 - \lambda_n},$$

and

$$C_n = \frac{V_{n\tilde{0}}}{\lambda_0 - \lambda_n}, \quad C'_n = \frac{V_{n'\tilde{0}}}{\lambda_0 - \lambda_n},$$

where

$$V_{n\tilde{0}} = C_0 \times \begin{cases} \dfrac{3\sqrt{-\pi D}}{2} - \dfrac{3R_U}{4}, & n = 1; \\ \dfrac{2n+1}{n(n+1)}\dfrac{(-1)^n R_U}{2}, & n \geqslant 2. \end{cases}$$

$$V_{n'\tilde{0}} = C_0 \times \left\{ -\frac{2n+1}{n(n+1)}\frac{(-1)^n R_U}{\sqrt{\pi}}, \quad n \geqslant 1. \right.$$

$$V_{\tilde{0}n} = C_0 \times \left\{ -\frac{2n+1}{n(n+1)}\frac{(-1)^n R_U}{2}, \quad n \geqslant 1. \right.$$

$$V_{\tilde{0}n'} = C_0 \times \begin{cases} \dfrac{\pi\sqrt{-D}}{4} - \dfrac{3R_U}{2\sqrt{\pi}}, & n = 1; \\ \dfrac{2n+1}{n(n+1)}\dfrac{(-1)^n R_U}{\sqrt{\pi}}, & n \geqslant 2. \end{cases}$$

Using the fact that

$$\sum_{n=2}^{\infty}\frac{(2n+1)^2}{2n^3(n+1)^3} = -\frac{25}{16} + \frac{\pi^2}{6},$$

we find

$$\gamma_2 = \frac{3R_U}{4\sqrt{\pi}(\pi+4)} + \frac{R_U^2}{2\pi^2}\left(1 - \frac{\pi^2}{6}\right).$$

For the eigenfunction, we obtain

$$\sum_{n=1}^{\infty}(C_n\boldsymbol{b}_n + C_n'\boldsymbol{b}_n') = \frac{C_0}{\pi^2}\left\{\frac{3}{4}\left[\sqrt{-\pi D}\boldsymbol{b}_1 - \frac{R_U}{2}\left(\boldsymbol{b}_1 - \frac{2\boldsymbol{b}_1'}{\sqrt{\pi}}\right)\right] + \frac{R_U}{2}\sum_{n=2}^{\infty}\left[\frac{(-1)^n(2n+1)}{n^2(n+1)^2}\left(\boldsymbol{b}_n - \frac{2\boldsymbol{b}_n'}{\sqrt{\pi}}\right)\right]\right\}.$$

Thus, the final solution of second order perturbation theory, upon restoring $\epsilon = 1$, and also restoring the original definitions of $\mathcal{B}_r$ and $\mathcal{B}_\phi$ in equation (A3), reduces to

$$\gamma = -\frac{\pi^2}{4} + \frac{\sqrt{-\pi D}}{2} - \frac{R_U}{2} + \frac{3\sqrt{-\pi D}R_U}{4\pi(\pi+4)} + \frac{R_U^2}{2\pi^2}\left(1 - \frac{\pi^2}{6}\right),$$

$$\mathcal{B}_r = C_0 R_\alpha\left\{\cos\left(\frac{\pi z}{2}\right) + \frac{3}{4\pi^2}\left(\sqrt{-\pi D} - \frac{R_U}{2}\right)\cos\left(\frac{3\pi z}{2}\right) + \frac{R_U}{2\pi^2}\sum_{n=2}^{\infty}\frac{(-1)^n(2n+1)}{n^2(n+1)^2}\cos\left[\left(n+\tfrac{1}{2}\right)\pi z\right]\right\}, \quad \text{(A5)}$$

$$\mathcal{B}_\phi = -\frac{2}{\pi}C_0\sqrt{-\pi D}\left\{\cos\left(\frac{\pi z}{2}\right) - \frac{3R_U}{8\pi^2}\cos\left(\frac{3\pi z}{2}\right) + \frac{R_U}{2\pi^2}\sum_{n=2}^{\infty}\frac{(-1)^n(2n+1)}{n^2(n+1)^2}\cos\left[\left(n+\tfrac{1}{2}\right)\pi z\right]\right\}, \quad \text{(A6)}$$

where $C_0 = 1/\sqrt{1+4/\pi}$ for the solution normalized as $\int_0^1 B^2 dz = 1$. The eigenfunctions are plotted in Fig. A1 and the magnetic pitch angle, in Fig. A2. Solving for the critical ($\gamma = 0$) dynamo number we obtain

$$D_{\rm c} = -\frac{\pi^3}{4}\left\{\frac{1 + 2R_U/\pi^2 - (2R_U^2/\pi^4)(1-\pi^2/6)}{1 + 3R_U/[2\pi(\pi+4)]}\right\}^2.$$

APPENDIX B: THE NO-z ASYMPTOTIC SOLUTION

Equations (8)-(10) can be solved in an approximate way as a set of algebraic equations by setting time derivatives to zero (that is, by assuming the system reaches a steady state) and by using the no-z approximation to replace z-derivatives by simple divisions. This method allows for a determination of all relevant quantities, but these quantities now represent averages over the disc half-thickness h. The method is not new (Sur et al. 2007), but here we neglect Ohmic terms, include the diffusive flux, and do not assume that $\overline{B}_r^2/\overline{B}_\phi^2 \ll 1$. We do, however, adopt the $\alpha\Omega$ approximation for simplicity. We also include an expression for the growth rate γ in the kinematic regime, which is obtained by assuming $\overline{\boldsymbol{B}} \propto {\rm e}^{\gamma t}$.

Furthermore, we include as yet unspecified numerical factors in the no-z terms. There are in general four such factors that are not already specified in Phillips (2001): $C_{U,r}$, such that $\partial(\overline{U}_z\overline{B}_r)/\partial z \simeq C_{U,r}\overline{U}_z\overline{B}_r/h$, $C_{U,\phi}$, where, similarly, $\partial(\overline{U}_z\overline{B}_\phi)/\partial z \simeq C_{U,\phi}\overline{U}_z\overline{B}_\phi/h$, $C_{\rm a}$, where $\partial(\overline{U}_z\alpha_{\rm m})/\partial z \simeq C_{\rm a}\overline{U}_z\alpha_{\rm m}/h$ for the advective flux term, and finally $C_{\rm d}$, with $\partial^2\alpha_{\rm m}/\partial z^2 \simeq C_{\rm d}\alpha_{\rm m}/h^2$ for the diffusive flux

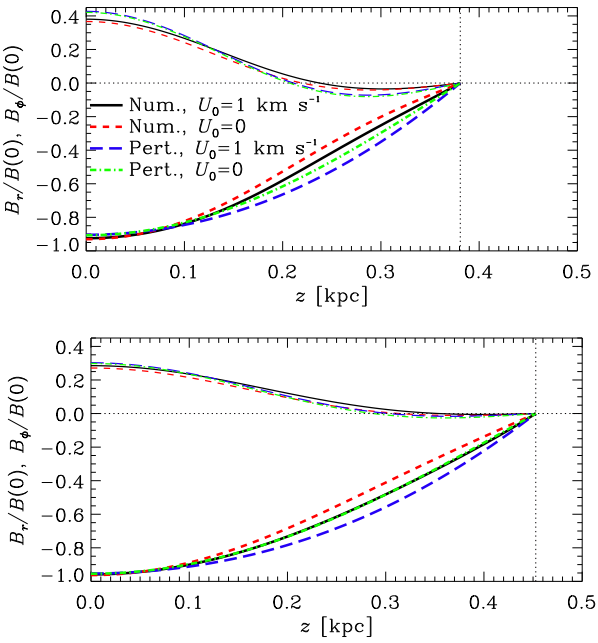

Figure A1. Radial (thin) and azimuthal (thick) components of $\overline{\boldsymbol{B}}$ in the kinematic stage, normalized to the magnetic field strength at the midplane for parameters corresponding to $r = 4\,$kpc (top) and $r = 8\,$kpc (bottom). Solutions from perturbation theory [equations (A5) and (A6)] are compared with numerical solutions for $U_0 = 0$ and $U_0 = 1\,{\rm km\,s^{-1}}$. Solutions are symmetric about the midplane.

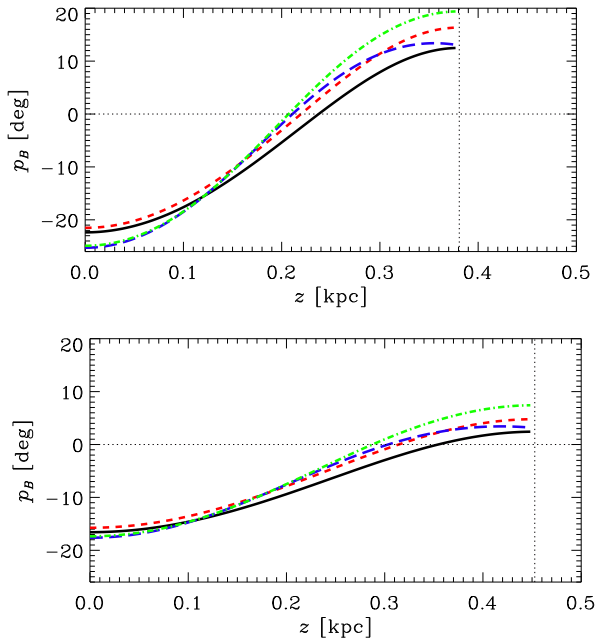

Figure A2. Magnetic pitch angle $p \equiv \arctan(\overline{B}_r/\overline{B}_\phi)$ in the kinematic stage, as a function of the distance z from the midplane, for parameters corresponding to $r = 4\,$kpc (top) and $r = 8\,$kpc (bottom). p is not plotted for $z = h$, as it is undefined at the disc boundaries, where the boundary conditions enforce $\overline{B}_r = \overline{B}_\phi = 0$. (See also Fig. A1.)

term. For simplicity, we approximate $C_{U,r} = C_{U,\phi} = C_U$, which turns out to be fairly reasonable (see Fig. B1 and the discussion in Section B1).

Equations (A1) and (A2) can be written in the no-z approximation, in dimensionless form ($h = \eta_{\rm t} = 1$) as

$$\left(\gamma + \frac{\pi^2}{4}g\right)\overline{B}_r = -\frac{2}{\pi}R_\alpha \overline{B}_\phi,$$
$$\left(\gamma + \frac{\pi^2}{4}g\right)\overline{B}_\phi = R_\omega \overline{B}_r,$$

where $g \equiv 1 + 4C_U R_U/\pi^2$. From the solvability condition for the homogeneous equations $(\gamma + \pi^2 g/4)^2 = -2D/\pi$, we set $\gamma = 0$ to obtain the critical dynamo number,

$$D_{\rm c} = -\frac{\pi^5}{32}g^2.$$

Solving for γ, we then obtain

$$\gamma = \frac{\pi^2}{4}t_{\rm d}^{-1} g\left(\sqrt{\frac{D}{D_{\rm c}}} - 1\right),$$

where $t_{\rm d} = h^2/\eta_{\rm t}$ is the turbulent diffusion time-scale. Defining $p \equiv \arctan(\overline{B}_r/\overline{B}_\phi)$, and letting $R_\alpha = R_{\alpha,{\rm c}}$ since we are interested in the saturated solution, we obtain

$$\tan p = \sqrt{-\frac{2R_{\alpha,{\rm c}}}{\pi R_\omega}} = \frac{\pi^2}{4}\frac{g}{R_\omega}. \qquad \text{(B1)}$$

Finally, for the saturation field strength we use equation (10) with the left hand side equal to zero, the expression

$$(\boldsymbol{\nabla}\times\overline{\boldsymbol{B}})\cdot\overline{\boldsymbol{B}} \simeq -\frac{3\sqrt{-\pi D_{\rm c}}\tan(p)B^2}{8h[1+\tan^2(p)]} \qquad \text{(B2)}$$

valid in the no-z approximation (Sur et al. 2007), along with the above expression (B1) for $\tan p$ in terms of $R_{\alpha,{\rm c}}$. It is then straightforward to obtain

$$B^2 = B_{\rm eq}^2\frac{\xi(p)}{C}\left(\frac{D}{D_{\rm c}} - 1\right)\left(C_{\rm a}R_U - C_{\rm d}R_\kappa\right),$$

where $\xi(p) \equiv [1 - 3\cos^2(p)/(4\sqrt{2})]^{-1}$ and $C \equiv 2(h/l)^2$. We note that $C_{\rm d} < 0$ (Section B1).

B1 Refining the no-z approximation

The values of C_U, $C_{\rm a}$ and $C_{\rm d}$ are estimated in the following way. To estimate C_U, equations (8) and (9) are first solved numerically and the true value of the growth rate γ obtained. The no-z approximation is then applied *to only those terms involving* C_U, e.g. $\partial(\overline{U}_z\overline{B}_r)/\partial z$ is replaced with $C_U U_0 \overline{B}_r/h$ (but $\overline{B}_r$ is still z-dependent). The value of C_U is then varied iteratively until γ is equal to the true value. This is also done for $C_{U,r}$ and $C_{U,\phi}$ by using the method on each of the relevant terms, individually. To estimate $C_{\rm a}$ and $C_{\rm d}$, the same approach is taken, with the relevant term involving $C_{\rm a}$ or $C_{\rm d}$ replaced with its no-z form, but now equations (8)-(10) are solved, and instead of matching the growth rate,

$$\langle B\rangle \equiv \frac{1}{2h}\int_{-h}^{h} B dz,$$

is matched to its true value. Alternatively, $\langle B^2\rangle^{1/2}$ could be chosen, but it was found that this choice leads to very similar results.

The results are summarized in Fig. B1. Unfortunately, C_U, represented by circles in the left panel, has a fairly strong dependence on D, but luckily, a rather weak dependence on R_U. We adopt the value $C_U = 0.25$, which seems to be a reasonable choice given the data. The middle panel shows the values of $C_{\rm a}$ obtained for different D, R_U and R_κ. Values are close to unity for $R_\kappa = 0$, but drop quite drastically when $R_\kappa = 0.3$. We adopt $C_{\rm a} = 1$, keeping in mind that for cases with both advective and diffusive flux, this is an overestimate. Finally, the results for $C_{\rm d}$ are illustrated in the right panel of Fig. B1. Its value does not stray very far from $-\pi^2$, which is the value that would be obtained if $\alpha_{\rm m}$ were sinusoidal in z.

We therefore adopt the values $C_U = 1/4$, $C_{\rm a} = 1$, and $C_{\rm d} = -\pi^2$ in the present work. It is worth mentioning that these choices may not be as suitable for a different $\overline{U}_z$ profile. With these choices, approximating a given term by its no-z form leads to errors in quantities such as γ, $\langle B/B_{\rm eq}\rangle$ or the pitch angle p of typically $< 10\%$ for parameters corresponding to $r = 4\,$kpc or $r = 8\,$kpc in our model. We fully realize that the values of these numerical factors, and the method used to determine them, are not exact or unique; the idea is to improve the no-z approximation in the same spirit as Phillips (2001), while admitting that the approximation itself is rather crude by nature.

REFERENCES

Bardou A., von Rekowski B., Dobler W., Brandenburg A., Shukurov A., 2001, A&A, 370, 635
Beck R., 2007, A&A, 470, 539
Beck R., Brandenburg A., Moss D., Shukurov A., Sokoloff D., 1996, ARA&A, 34, 155
Bernet M. L., Miniati F., Lilly S. J., 2013, ApJ, 772, L28
Blackman E. G., 2014, ArXiv e-prints
Blackman E. G., Field G. B., 2000, ApJ, 534, 984
Brandenburg A., 2003, Computational aspects of astrophysical MHD and turbulence, Taylor & Francis, London, p. 269
Brandenburg A., Candelaresi S., Chatterjee P., 2009, MNRAS, 398, 1414
Brandenburg A., Subramanian K., 2005, PhR, 417, 1
Chamandy L., Subramanian K., Quillen A., 2014, MNRAS, 437, 562
Chamandy L., Subramanian K., Shukurov A., 2013a, MNRAS, 428, 3569
—, 2013b, MNRAS, 433, 3274
Chyży K. T., Buta R. J., 2008, ApJ, 677, L17
Ebrahimi F., Bhattacharjee A., 2014, ArXiv e-prints
Elstner D., 2005, in The Magnetized Plasma in Galaxy Evolution, Chyzy K. T., Otmianowska-Mazur K., Soida M., Dettmar R.-J., eds., Jagiellonian University, Krakow, pp. 117–124
Fletcher A., 2010, in Astron Soc Pacific Conf Ser, Kothes R., Landecker T. L., Willis A. G., eds., Vol. 438, p. 197
Frick P., Beck R., Shukurov A., Sokoloff D., Ehle M., Kamphuis J., 2000, MNRAS, 318, 925
Gressel O., Bendre A., Elstner D., 2013, MNRAS, 429, 967
Griffiths D., 2005, Introduction to Quantum Mechanics. Pearson Education, Essex

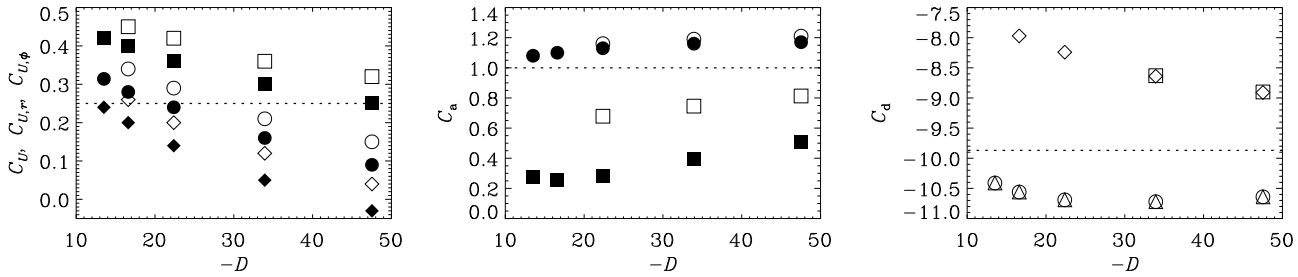

Figure B1. Left: Parameter C_U for $U_0 = 1\,\mathrm{km\,s^{-1}}$ (filled circles) and $2\,\mathrm{km\,s^{-1}}$ (open circles), $C_{U,r}$ for $U_0 = 1\,\mathrm{km\,s^{-1}}$ (filled diamonds) and $2\,\mathrm{km\,s^{-1}}$ (open diamonds), $C_{U,\phi}$ for $U_0 = 1\,\mathrm{km\,s^{-1}}$ (filled squares) and $2\,\mathrm{km\,s^{-1}}$ (open squares). Middle: Parameter C_a for $U_0 = 1\,\mathrm{km\,s^{-1}}$ and $R_\kappa = 0$ (filled circles), $U_0 = 2\,\mathrm{km\,s^{-1}}$ and $R_\kappa = 0$ (open circles), $U_0 = 1\,\mathrm{km\,s^{-1}}$ and $R_\kappa = 0.3$ (filled squares), and $U_0 = 2\,\mathrm{km\,s^{-1}}$ and $R_\kappa = 0.3$ (open squares). Right: Parameter C_d for $R_\kappa = 0.3$ and $U_0 = 0$ (circles), $R_\kappa = 0.3$ and $U_0 = 1\,\mathrm{km\,s^{-1}}$ (diamonds), $R_\kappa = 0.3$ and $U_0 = 2\,\mathrm{km\,s^{-1}}$ (squares), and $R_\kappa = 0.6$ and $U_0 = 0$ (triangles). Data for five different dynamo numbers $D = -47.5, -33.9, -22.4, -16.6, -13.5$, corresponding to radii $r = 2, 4, 6, 8, 10\,\mathrm{kpc}$, respectively, is shown. Chosen values $C_U = 0.25$, $C_\mathrm{a} = 1$ and $C_\mathrm{d} = -\pi^2$ are shown by dashed lines on their respective graphs.

Gruzinov A. V., Diamond P. H., 1994, Phys Rev Lett, 72, 1651

Heald G. H., 2012, ApJ, 754, L35

Ji Y., Cole L., Bushby P., Shukurov A., 2013, ArXiv e-prints 1312.0408

Kleeorin N., Moss D., Rogachevskii I., Sokoloff D., 2000, A&A, 361, L5

—, 2002, A&A, 387, 453

Kleeorin N., Rogachevskii I., Ruzmaikin A., 1995, A&A, 297, 159

Kleeorin N., Ruzmaikin A. A., 1982, Magnetohydrodynamics, 18, 116

Krause F., Rädler K.-H., 1980, Mean-field Magnetohydrodynamics and Dynamo Theory. Pergamon Press, Oxford

Kulsrud R. M., Zweibel E. G., 2008, Rep on Prog Phys, 71, 046901

Mitra D., Candelaresi S., Chatterjee P., Tavakol R., Brandenburg A., 2010, Astron Nachr, 331, 130

Moffatt H. K., 1978, Magnetic Field Generation in Electrically Conducting Fluids. Cambridge Univ Press, Cambridge

Moss D., 1995, MNRAS, 275, 191

—, 1998, MNRAS, 297, 860

Moss D., Beck R., Sokoloff D., Stepanov R., Krause M., Arshakian T. G., 2013, A&A, 556, A147

Moss D., Shukurov A., Sokoloff D., 1999, A&A, 343, 120

—, 2000, A&A, 358, 1142

Phillips A., 2001, Geophys Astrophys Fluid Dyn, 94, 135

Pouquet A., Frisch U., Leorat J., 1976, Journal of Fluid Mechanics, 77, 321

Rädler K.-H., Kleeorin N., Rogachevskii I., 2003, Geophys Astrophys Fluid Dyn, 97, 249

Rohde R., Beck R., Elstner D., 1999, A&A, 350, 423

Ruzmaikin A. A., Shukurov A. M., Sokoloff D. D., 1988, Magnetic Fields of Galaxies. Kluwer, Dordrecht

Ruzmaikin A. A., Turchaninov V. I., Zeldovich I. B., Sokoloff D. D., 1979, Ap&SS, 66, 369

Shukurov A., 1998, MNRAS, 299, L21

—, 2005, in Lecture Notes in Physics, Berlin Springer Verlag, Vol. 664, Cosmic Magnetic Fields, Wielebinski R., Beck R., eds., p. 113

—, 2007, Mathematical Aspects of Natural Dynamos, Dormy E., Soward A. M., eds., Chapman & Hall/CRC, London, pp. 313–359

Shukurov A., Sokoloff D., 2008, in Les Houches, Vol. 88, Dynamos, Cardin P., Cugliandolo L. F., eds., Elsevier, pp. 251–299

Shukurov A., Sokoloff D., Subramanian K., Brandenburg A., 2006, A&A, 448, L33

Subramanian K., Brandenburg A., 2006, ApJ, 648, L71

Subramanian K., Mestel L., 1993, MNRAS, 265, 649

Sur S., Shukurov A., Subramanian K., 2007, MNRAS, 377, 874

Tabatabaei F. S., Krause M., Fletcher A., Beck R., 2008, A&A, 490, 1005

Vainshtein S. I., Cattaneo F., 1992, ApJ, 393, 165

Vishniac E. T., Cho J., 2001, ApJ, 550, 752

Vishniac E. T., Shapovalov D., 2014, ApJ, 780, 144